Enhancing Gas Absorption with Nanoengineered Surfaces for Bubble Manipulation

By

Tal Joseph

B.S. Chemical Engineering
Yale University, 2021

Submitted to the Department of Mechanical Engineering
in Partial Fulfillment of the
Requirements for the Degree of

Master of Science in Mechanical Engineering

at the

Massachusetts Institute of Technology

June 2023

Authored by: Tal Joseph
Department of Mechanical Engineering
May 12, 2023

Certified by: Kripa K. Varanasi
Professor of Mechanical Engineering, Thesis Supervisor

Accepted by: Nicolas Hadjiconstantinou
Chairman, Committee on Graduate Students

Enhancing Gas Absorption with Nanoengineered Surfaces for Bubble Manipulation

By

Tal Joseph

Submitted to the Department of Mechanical Engineering on May 12, 2023
in Partial Fulfillment of the
Requirements for the Degree of

Master of Science in Mechanical Engineering

ABSTRACT

Efficiently reacting gases with liquid absorbents is a crucial aspect of numerous industrial processes on a large scale. When the gas phase is in the form of discrete bubbles within an absorber unit, such as in bubble column absorbers or gas sparging systems, the effectiveness of these bubbles' reaction depends on carefully controlling their properties and flow. This study demonstrates the efficacy of a novel method for gas absorption into a liquid absorbent, which involves using nanoengineered surfaces to spread bubbles into their texture and enhance mass transport between the gas and liquid phases. This surface-enhanced direct injection approach for gas absorption yields more than a two-order-of-magnitude improvement in reaction rate compared to captive bubbles when using a moderately alkaline potassium hydroxide as an absorbent solution for carbon dioxide gas. While the average reaction rates of non-spreading bubbles typically decrease with bubble size, the surface-enhanced absorption of spreading bubbles reverses this trend, enabling the most rapid absorption for the smallest bubbles. Moreover, non-spreading carbon dioxide bubbles cannot be fully absorbed due to product aggregation at their interface, whereas spreading bubbles can avoid this regime by reacting more quickly than the aggregation process on rapid timescales. Finally, we propose this surface-enhanced direct injection method as an absorption technique that scales advantageously for small-scale or distributed modular absorber designs compared to the traditional large-scale absorber units currently used in industry.

Thesis Supervisor: Kripa K. Varanasi
Title: Professor of Mechanical Engineering

Acknowledgements

First, I would like to thank my advisor, Professor Kripa Varanasi, for his valuable guidance and support. In the short period of time that I have worked with him, I have learned more than I could ever imagine. His knowledge, motivation, creativity, passion, and kindness have been a constant source of inspiration for me. I am excited to continue working with him as my mentor for my doctoral studies.

I would like to thank all the members of the Varanasi Lab, including Simon, Bert, Sean, Saurabh, Fabian, Tess, Caroline, Rafael, and Mike, for their unwavering help, advice, discussion, and guidance. Each of you has not only influenced my work but also contributed to my personal growth. I eagerly look forward to tackling more interesting problems alongside all of you in the years to come. It is truly an honor to be part of such an incredible team.

I would like to wholeheartedly express my deepest gratitude to Dafna, my incredible partner, for her unwavering support and assistance throughout my academic journey. Her constant encouragement, understanding, and patience have been the pillars of strength that helped me overcome the many challenges I faced along the way. Dafna's invaluable presence has provided me with the motivation and resilience needed to navigate this arduous path, and I am genuinely thankful for the role she has played in my achievements. I am confident in saying that I could not have come this far without her unwavering love and support. Thank you, Dafna, for being the rock upon which I have built my accomplishments.

I am deeply grateful to my family for their support, love, and encouragement during my pursuit of a master's degree. I would like to express my heartfelt appreciation to my parents, Orly and Eylon, my twin brother Daniel, my younger brother Shahar, and my grandmother Naomi, who have all provided me with the tools, advice, and support I needed throughout my upbringing and academic journey. Their collective guidance has been invaluable in helping me achieve my goals. I am especially thankful to Daniel, who took it upon himself to manage our family business and lead it to success, all while understanding and respecting my academic commitments without harboring any resentment.

Table of Contents

List of Figures

List of Tables

INTRODUCTION

The uptake of gaseous substances into aqueous media has numerous crucial applications in various industries. A common method for achieving this is through the employment of absorbers, which represent a standard unit operation in chemical engineering for separation processes, encompassing different gas/liquid contactor types such as packed towers, spray columns, and bubble column varieties, among others[1]. The objective of these absorption techniques is to maximize the interaction between the gas and liquid phases in order to facilitate better mass transport. Absorption towers, for instance, are frequently utilized to eliminate potentially harmful gases from being discharged into the atmosphere during industrial processes. Packed tower absorbers serve a range of chemical scrubber applications, including the removal of NO_x[2], as well as the absorption of carbon dioxide [3] and ammonia gases[4]. The operational intricacies of various absorption units, along with their underlying principles and design parameters, have been thoroughly documented in several textbooks [5].

In specific types of reactive absorber units, such as bubble column absorbers, the gas phase predominantly exists as discrete bubbles rather than as a bulk gas phase interacting with thin liquid absorbent films[1]. Consequently, the direct injection of bubbles into reactors that readily react with the surrounding liquid media is a widely adopted practice across numerous industries to enhance mass transport between gas and liquid phases. Nonetheless, in certain applications, the formation of foams resulting from bubble injection can be detrimental and cause problems. For example, in sparged gas systems for bioreactor operation, foams can decrease reactor yield[6] and even lead to cell death upon bubble rupture [7,8]. The use of spargers for aeration in fermenters and bioreactors is also essential for the cultivation of bacteria and algae in various bioreactor types, including photobioreactors and miniature bioreactors[9–11] As a result, mitigating foam generation using

defoamer additives to minimize these adverse effects has become a multi-billion-dollar market with continued growth [12]. Additionally, gas sparging for dissolution into liquid plays a vital role in food industry processes, such as beverage aeration[13], and as a pre-processing step in water treatment using injected bubbles to facilitate the removal of solid particles and oils [14,15] as well as membrane antifouling in submerged anaerobic membrane reactors (SAMBRs) for sewage treatment [16,17].

In light of the global scientific and engineering community's commitment to advancing technologies that address climate change and promote sustainable energy solutions, the absorption of carbon dioxide (CO_2) has become an especially significant system to investigate due to the central role CO_2 plays in climate change and future sustainability considerations. Accordingly, the model system examined in this work involves the absorption of CO_2 gas in an alkaline aqueous solution of potassium hydroxide with moderate ionic strength. Previous extensive research on CO_2 bubble absorption in various alkaline solutions offers valuable references for physical constants and prior experimental findings for comparison purposes[18–20]. Furthermore, the capture[21,22], conversion[23] and storage/utilization[24] of carbon dioxide poses a critical contemporary challenge, with numerous approaches being proposed. Traditional methods of chemical absorption and physical adsorption are common strategies for CO_2 separation from both dilute and concentrated streams[25] Recently, innovative and promising electrochemical techniques for carbon dioxide separations have also been demonstrated[26].

From a carbon storage perspective, CO_2 mineralization efforts encompass a broad array of methods and applications[27,28] including CO_2 mineralization using waste streams[29,30], saline sources like ocean water[31], and injection of CO_2 into geologic formations[32]. For instance, CO_2 mineralization in geological formations currently occurs on relatively large scales, such as in the

Sleipner Field off the coast of Norway in the North Sea[33], with approximately 1 Mt of CO_2 injection annually, as well as in newer pilot-scale facilities like the CarbFix project in Iceland [34–36]. However, the processes associated with this type of underground storage transpire over geological timescales, requiring many years for the mineralization reaction to complete and fix the carbon dioxide into a mineralized form. For example, recent results published by the CarbFix team indicate that nearly 200 tonnes of CO_2 injected at depth were almost entirely mineralized after approximately two years[37]. The wettability of rock formations into which CO_2 is injected has crucial implications for permeability and mineralization dynamics, as well as storage capacity when carbon is sequestered in this manner, such as in deep saline aquifers[38]. However, the wettability of any solid surface in contact with a gas targeted for absorption also has significant consequences in traditional absorbers, like packed tower absorbers. In these packed tower configurations, the packing materials are typically coated to promote the wetting of the liquid absorbent, thereby creating a continuous film and establishing the interface upon which the target gas is absorbed[1]. The research presented here aims to engineer surfaces that exhibit advantageous benefits for spreading CO_2 gas bubbles into their textures, thereby promoting enhanced absorption into an alkaline media that is less wetting to the surface than the gas. In this manner, capillary forces can be used advantageously to spread the bubble to be absorbed and improve mass transport between the gas and liquid phases compared to a bubble rising in the liquid media, as is the case in a bubble column type absorber.

To achieve this goal, engineered superhydrophobic surfaces will be developed to spread bubbles and enhance mass transport through advantageous geometric manipulation of bubbles via capillary forces. Prior work has thoroughly analyzed the dynamics of spreading air bubbles' fundamentals, but these bubbles did not readily react with the surrounding liquid media[39].

Moreover, research on bubble capture has employed similar surfaces for the rapid spreading of bubbles into capture surfaces to prevent foam accumulation at free interfaces for industrial applications[40]. Again, this study presents a method for the removal and mitigation of foam accumulation and does not investigate a readily reacting gas/liquid system. To the best of our knowledge, no work has yet been published that examines spreading bubbles on nanoengineered surfaces with a bubble that rapidly reacts with the surrounding liquid media. In this study, we present a system that enhances the reaction rates of CO_2 relative to plain bubble reaction rates by spreading the gas into nanoengineered capture surfaces. While the system presented here is motivated towards developing an absorber system uniquely suited for small-scale and distributed CO_2 absorption applications for sustainability, the results are relevant for any gas/liquid absorption system and have general relevance for other chemical reactions for absorption.

RESULTS AND DISCUSSION

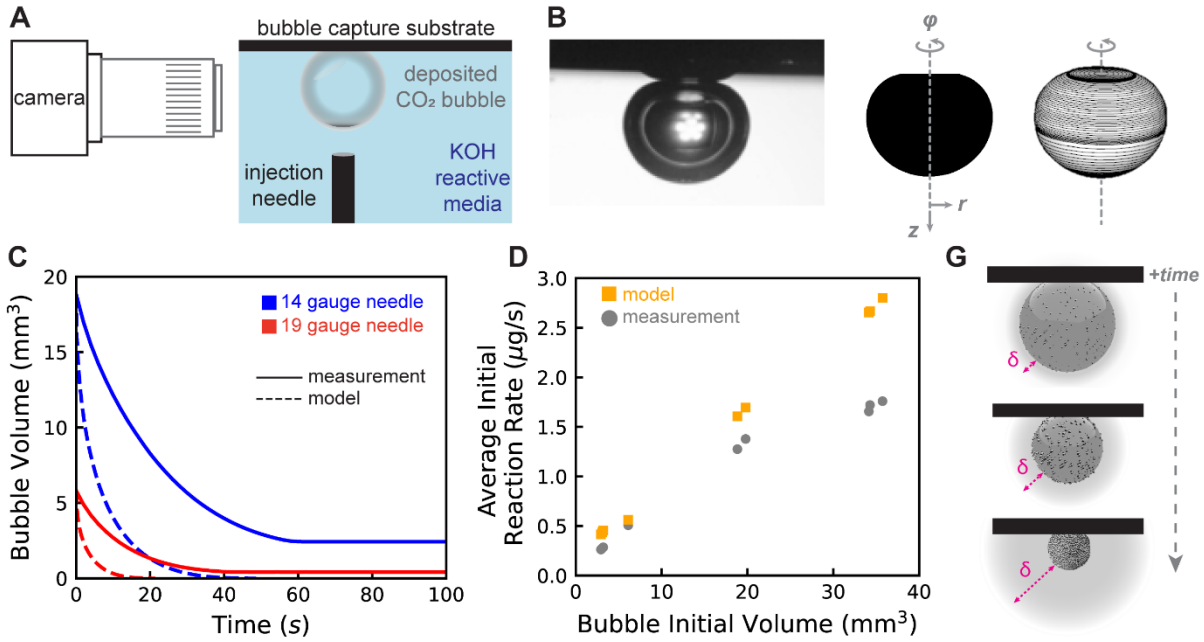

Figure 1. (A) Experimental setup for capturing side-profile images of CO_2 bubbles during absorption over time in 0.1 M KOH absorbate. (B) A representative image acquired during data collection, followed by binary conversion of the bubble image, enabling rotation of the 2D image around its approximate axis of symmetry to compute the bubble volume as a function of time. (C) A graph displaying the change in bubble volume due to absorption over time for two distinct CO_2 bubble sizes introduced by varying dispensing needle sizes, depicted in different colors. Solid lines represent direct measurements, while dotted lines indicate predictions based on the developed analytical model. (D) A plot illustrating the average initial reaction rate observed during the first 20 seconds for the tested bubble sizes, along with the corresponding predicted average reaction rates for the same period as projected by the model. (G) A visual representation of two processes occurring as time progresses for a captured bubble during experiments. Firstly, the mass diffusion boundary (denoted in pink by δ) expands over time. Secondly, reacted particles accumulate at the interface until they eventually cause the bubble absorption to plateau, halting the reaction.

Experimentally Determining the Rate of CO_2 Absorption

In order to establish a baseline for quantifying the evolution of gas bubble absorption, a setup was developed to image the captured bubbles from a side profile (Figure 1A). Single bubbles of pure CO_2 gas were delivered to the submerged capture surface in 0.1 M KOH using stainless steel dispensing needles. Detailed information about the experimental setup and the single bubble delivery system can be found in the supporting information (refer to SI §4 for more experimental

setup details). Once the bubbles were rapidly deposited, videos were recorded to document the absorption evolution, and image processing techniques were used to extract the volume changes of the bubbles during their reaction with KOH throughout the experiments (Figure 1B). The resulting data was analyzed to determine the reaction rates for the CO_2 bubbles' absorption in the KOH solution (see SI §2 for additional image processing detail).

As illustrated in Figure 1C, the data collected from the experiments reveals two interesting characteristics of the dissolution process for captured bubbles on a hydrophilic capture surface. Here, the bubbles remain relatively spherical in shape throughout the absorption process. First, the reaction rates for bubbles of different sizes, which are achieved by changing the diameter of the dispensing needle, decrease over time. Second, after about 40 seconds for the smaller bubble (red trace) and approximately 60 seconds for the larger bubble (blue trace), the absorption process stops, and the size of the bubbles plateaus, with no further absorption occurring. Both of these features, the decrease in flux over time and the plateauing behavior, have been previously reported and are consistent with the observations made in this study[19,41–43]. The decrease in flux at the bubble's interface is due to the growth of the diffusion boundary layer, graphically shown in Figure 1E. The plateauing behavior of bubbles is most likely attributable to the accumulation of reaction products at the interface, also depicted in Figure 1E. As the bubbles decrease in size, the interfacial area where these particulates reside increases, and eventually, their presence effectively passivates the interface, preventing further reaction. For much higher concentrations of hydroxide solutions, it has been previously observed that a visible and solid shell will rapidly form around the CO_2 gas bubble, also stopping the reaction from continuing[19]. A numerical model was developed to capture the mass transport phenomena occurring for an idealized case of a spherical bubble of a certain volume being absorbed in a hydroxide solution. This model was created to compare against the

experimental results for bubbles of various sizes deposited onto a smooth silicon substrate, which serves as an analog for a stagnant bubble being absorbed in a solution. The reaction-diffusion model's details will be summarized in a subsequent section.

In Figure 1C, the dotted traces of different colors represent the model's prediction of the evolution of gas absorption for the tested bubbles. The model predicts higher rates throughout the bubble's absorption due to the simplification that the spherical bubble does not have the capture surface impeding KOH access and limiting some portion of the bubble's surface area. The model also predicts that the bubbles are completely absorbed by the hydroxide solution, which is expected as the secondary aggregation of reaction products on the interface is not included in the model. However, the primary aim of the numerical model is to accurately predict the order of magnitude of reaction rates for the bubbles being tested, as we aim to substantially decrease the timescale for these bubbles to be absorbed by engineering the capture surface to promote enhanced mass transport via spreading the gas into the superhydrophobic surface texture. For a larger bubble with an initial volume of approximately 18 mm3, the predicted absorption time is about 45 seconds, while a smaller bubble of approximately 6 mm3 takes roughly 20 seconds to be completely absorbed. The explicit goals of this work are twofold: (1) to decrease the absorption timescale for CO_2 bubbles, like those tested, to the order of milliseconds rather than tens of seconds, and (2) to enable the complete absorption of these gas bubbles, avoiding the plateauing behavior observed in the initial experiments. In the next section, we will discuss the numerical model that allows us to predict and compare empirical results for the tested conditions for the remainder of the experiments.

Numerically Simulating the Rate of CO_2 Bubble Absorption

A reaction-diffusion numerical model was created to enable the prediction of reaction rates and timescales associated with the complete absorption of CO_2 spherical bubbles suspended on the capture surface in KOH solution. This model serves as a point of comparison with relatively spherical bubbles deposited onto hydrophilic surfaces, such as those depicted in Figure 1. Furthermore, the model will also help in predicting the fully spreading bubble case for comparison, which will be showcased in a later section. As previously mentioned, the primary focus of the numerical model is to predict the order of magnitude of reaction rates rather than achieving extremely high levels of accuracy. It also serves as a tool to estimate what we should expect from a spreading bubble system from an order of magnitude standpoint.

In the modeled system for the chemical absorption under investigation, KOH and CO_2 undergo the following irreversible reaction, with k representing the reaction rate coefficient for the reaction:

$$KOH + CO_2 \overset{k}{\rightarrow} KHCO_3$$

The conservation of mass equations for OH^- and CO_2 govern the system's dynamics. Assuming a stationary bubble boundary (based on the quasi-stationary assumption), we disregard the advective transport term in the conservation equations, resulting in a reaction-diffusion system. Consequently, we solve a pair of interconnected partial differential equations numerically.

$$\frac{\partial c_{CO_2}}{\partial t} = D_{CO_2}\nabla^2 c_{CO_2} - k c_{CO_2} c_{OH^-}$$

$$\frac{\partial c_{OH^-}}{\partial t} = D_{OH^-}\nabla^2 c_{OH^-} - k c_{CO_2} c_{OH^-}$$

In this system, c_{CO_2} and c_{OH^-} represent the concentrations of carbon dioxide and hydroxide ions, respectively. D_{CO_2} and D_{OH^-} denote the diffusivities of carbon dioxide and hydroxide, respectively, while k represents the reaction rate coefficient and t stands for time. The system is solved by applying suitable boundary and initial conditions, as outlined in Table 1.

Table 1. Boundary and initial conditions applied in numerical modeling, where H denotes the Henry's Law constant for CO_2, c_{CO_2} and c_{OH^-} symbolize the concentrations of carbon dioxide gas and hydroxide ions in the system, respectively. Time is represented by the variable t, and r signifies the radial spatial variable in a spherical coordinate system. The bubble radius is indicated by R, while c_{Bulk,OH^-} represents the bulk concentration of hydroxide ions in the system, set at 0.1 M in this case.

Type	Condition
Boundary Conditions (4)	$c_{CO_2}(r = R) = \mathcal{H} P_{CO_2}$ $c_{OH^-}(r \rightarrow \infty) = c_{bulk,\,OH^-}$ $\frac{\partial c_{CO_2}}{\partial r}(r \rightarrow \infty) = 0$ $\frac{\partial c_{OH^-}}{\partial r}(r = R) = 0$
Initial Conditions (2)	$c_{CO_2}(r \geq R,\, t = 0) = 0$ $c_{OH^-}(r \geq R,\ t = 0) = c_{bulk,\,OH^-}$

To solve the system, we use the MATLAB pdepe function for both spherical and planar geometries, corresponding to non-spreading and spreading modeled cases. Concentration profiles are computed at each timestep, from which we determine the CO_2 flux [mol/m^2/s] at the surface and multiply it by the bubble's surface area to calculate the CO_2 bubble dissolution rate at each timestep [mol/s]. The bubble volume and surface area are continuously updated at each timestep, considering the remaining CO_2 in the bubble according to the ideal gas law.

Spatial and temporal mesh refinement were used to confirm convergence of bubble dissolution time for both spherical and planar geometries (refer to SI §3 for more information). The numerical CO_2 fluxes at 0.05 s and 10 s correspond well with the published textbook values for the same time intervals[19] (see SI §3 for comparison). Further details on numerical modeling, including a table of physical constants and material properties used in the numerical model, can be found in the supporting information section (see SI §3).

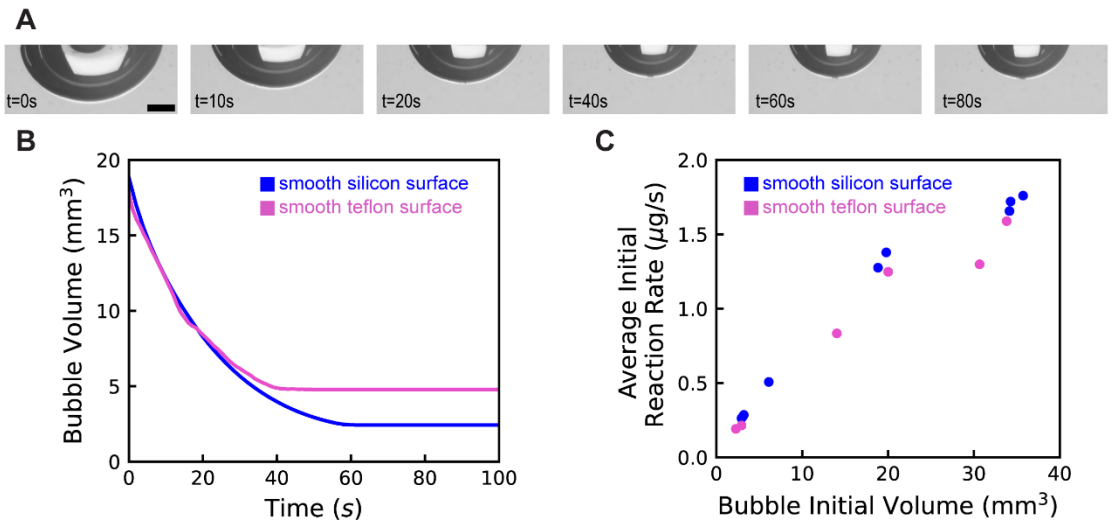

Figure 2. Investigating the influence of surface chemistry on the absorption dynamics of CO_2 in KOH. (A) Time-lapse images of a CO_2 bubble deposited onto a smooth hydrophobic PTFE (Teflon) surface to increase its surface area relative to its volume. (B) A graph illustrating the change in bubble volume due to absorption over time for two bubbles of equal volume positioned on either a smooth silicon hydrophilic surface or a smooth PTFE hydrophilic surface, demonstrating that the absorption dynamics are essentially the same for the first approximately 25 seconds, and the plateauing behavior persists in both instances. (C) A plot depicting the average initial rate observed during the first 20 seconds for the various bubble sizes tested on both a smooth silicon hydrophilic surface and a smooth PTFE hydrophobic surface.

Modifying Surface Chemistry of Capture Surface to Enhance Absorption

By modifying the bubble capture surface's chemistry, we can alter the bubble's wettability on the surface, leading to its spreading due to the hydrophobic properties of PTFE (polytetrafluoroethylene), commonly known as Teflon, on the smooth surface. Figure 2A demonstrates that applying a hydrophobic PTFE coating to a smooth surface indeed causes the bubble to spread on the substrate. However, this change in the bubble's geometry does not significantly impact the absorption dynamics compared to a smooth hydrophilic surface, as depicted in Figure 2B. The gas volume reduction over time is nearly identical for both smooth silicon and smooth Teflon surfaces during the first 25 seconds of absorption. Furthermore, both smooth hydrophilic and hydrophobic surfaces display a plateauing effect where the CO_2 bubble ceases absorption and remains static without reacting with the surrounding medium. Figure 2C

summarizes the similarities in reaction rates for bubbles of varying sizes deposited on hydrophilic silicon or hydrophobic Teflon smooth capture surfaces. As shown, larger bubbles exhibit higher average reaction rates due to their increased surface area compared to smaller bubbles, which react more slowly due to their smaller surface area. These findings underscore the crucial need for a roughened surface combined with appropriate hydrophobic surface chemistry to achieve complete spreading of a captured bubble, as previously reported in bubble capture studies[40]. This drives us to design and test various micro- and nano-textured capture surfaces to identify a suitable capture surface that facilitates rapid and complete spreading of the deposited CO_2 bubble on the surface.

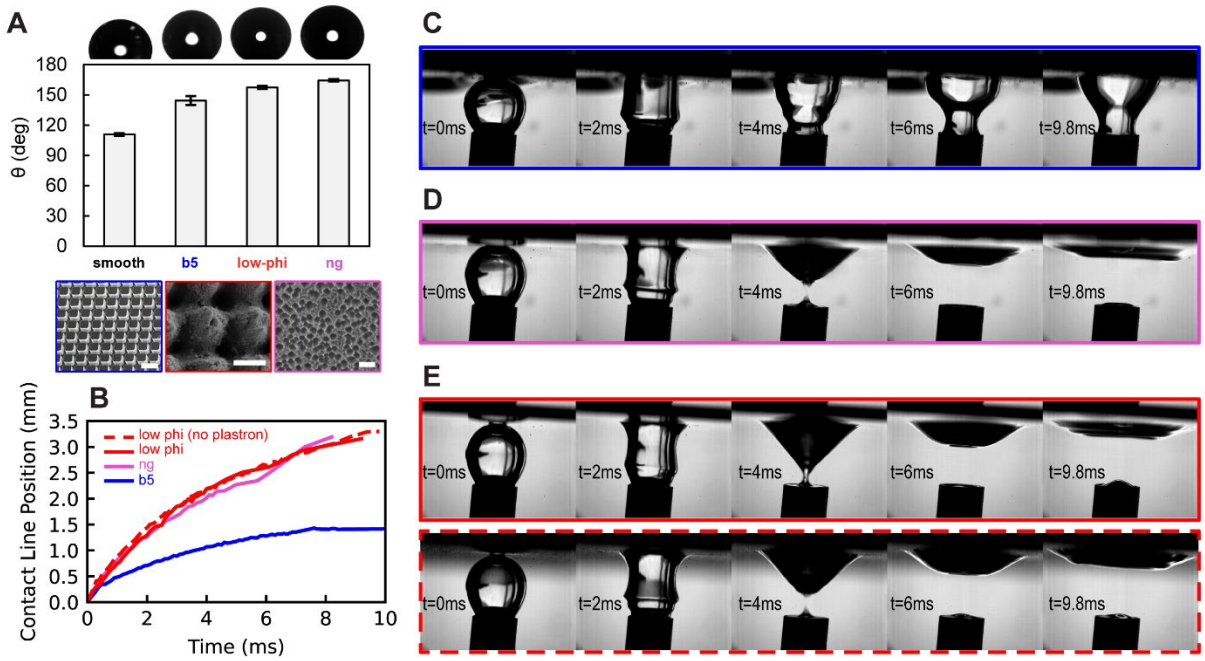

Figure 3. Developing surfaces that quickly and fully spread captured bubbles through their texture. (A) The top plot displays contact angle measurements for various tested capture surfaces using a water droplet to assess the wetting properties relevant to the KOH solution. The bottom section presents SEM micrographs of the three textured surfaces tested: the b5 micro-post surface in blue, the low-phi laser-ablated surface in red, and the reactive ion-etched "nano-grass" nanotextured surface in pink. (B) A graph illustrating the contact line motion over time for an air bubble brought to the surface of the tested capture surface while surrounded by non-reacting deionized water, highlighting the necessity of nanotexture for rapid and complete spreading, as well as the fact that a trapped gas layer is not required for this enhanced bubble capture to occur. (C-E) Time-lapse images from high-speed photography showing the evolution of the contact line for the b5 micro-post surface (C), the nano-grass surface (D), and the low-phi surface (E). In (E), both a low-phi surface with plastron (top) surrounded by a solid red line and without plastron (bottom) surrounded by a dashed red line are shown.

Rapid Gas Bubble Spreading on Nanoscale Superhydrophobic Surfaces

Surface roughness combined with hydrophobic surface chemistry is known to enable superhydrophobic surfaces with large equilibrium contact angles of 150º or more, as observed in nature and laboratory settings. Three distinct textured surfaces were created for testing bubble spreading capabilities: a microscale roughness micro-post array called "b5", a nanoscale roughness surface named "ng", and a hierarchical micro/nanoscale roughness surface designated as "low-phi" (Figure 3A). These textured surfaces were crafted on silicon wafers and silanized to produce hydrophobic surface chemistry. The fabrication process is described in more detail in the supporting information document (see SI §4). The equilibrium contact angles for these salinized

textured surfaces, along with an untextured salinized silicon substrate, are shown for comparison, highlighting the improvements achieved through texturing.

Subsequent experiments involved non-reactive bubbles spreading on these fabricated textures to assess their bubble spreading capabilities without considering reactivity. High-speed imagery was used to capture time-lapse photos of air bubbles in deionized water spreading over the surfaces within approximately 10 ms (Figure 3C-E). The b5 texture with microscale roughness, despite its large equilibrium contact angle, could not completely spread the bubble (Figure 3C). The bubble remained attached to the needle as the contact line was pinned to the surface and stopped spreading around 8 ms after being captured. In contrast, both the purely nanoscale ng texture and the hierarchical micro/nanoscale low-phi texture achieved complete spreading, detaching the air bubble from the needle and spreading the gas more rapidly than the microscale b5 texture (Figure 3D and 3E).

A final test confirmed that a thermodynamically stable 'plastron' layer of trapped air on superhydrophobic capture surfaces is not necessary for advantageous spreading dynamics. During experiments with reactive gas bubbles, the plastron layer had to be actively removed from capture surfaces before testing to visually track the dissolution of the captured gas layer. Spreading of an air bubble in deionized water on the hierarchical low-phi capture surface was tested with the plastron layer removed. The dynamics of bubble capture and spreading were similar for the low-phi surface with and without the plastron layer (Figure 3E), indicating the plastron layer is not essential for rapid and complete spreading in a reactive bubble case. By analyzing the images, we tracked the advancing front contact line of the captured air bubbles to measure velocity and compare dynamics between samples. As shown in Figure 3B, nanoscale textured surfaces exhibited similar spreading dynamics, while the purely microtextured capture surface spread the

captured bubble more slowly and pinned it before complete spreading. This emphasizes the need for nanoscale texture, as previously reported in studies on gas bubble capture with superhydrophobic surfaces[40]. Ultimately, the gathered data allowed us to estimate the spreading timescales for the bubbles, determined by the advancing contact line velocity during spreading. The microscale b5 texture exhibited instantaneous contact line velocities of up to 70 cm/s and an average velocity of 17 cm/s before being pinned. In contrast, the ng and low-phi surfaces (with or without a plastron) demonstrated similar spreading velocities, with instantaneous velocities reaching approximately 1.2 m/s and average velocities throughout the experiment around 36 cm/s, roughly twice that of the microscale b5 texture.

From the contact line velocities of the ng and low-phi surfaces, the spreading timescale for these bubbles was estimated to fall between 1 and 10 ms. This aligns with a scaling argument that balances the hydrostatic pressure, which drives the bubble into the texture, against the water's inertia, which resists the bubble's spreading. This balance results in a spreading timescale for bubbles in these cases scaling as $\tau_{spreading} \sim \frac{a^2}{(g\Omega)^{1/2}} \sim 10\ ms$, where a represents the capillary length (in our case, a ≈ 2.5 mm for water), g is the gravitational constant, and Ω is the spreading bubble's volume. This previously established timescale aligns well with our observed experimental results and previously reported contact line velocities of ~1 m/s for spreading air bubbles in water[39].

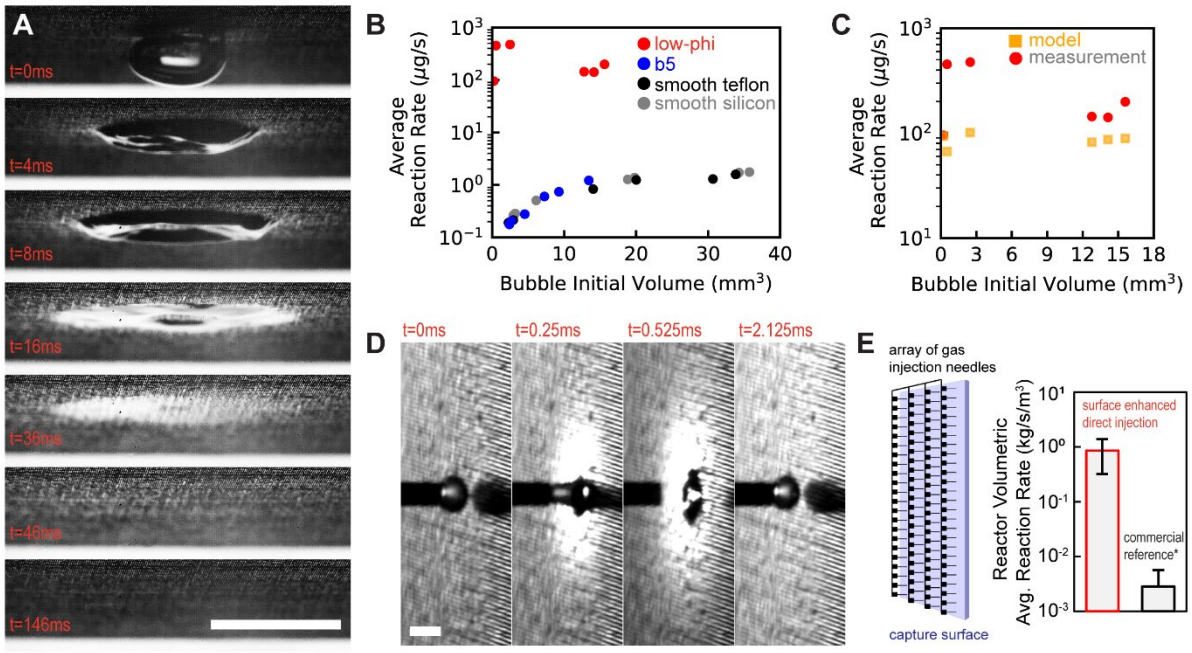

Figure 4. Rapid absorption of CO2 bubbles using a low-phi capture surface to increase reaction speeds and achieve full absorption. (A) Time-lapse images from high-speed cameras illustrating CO_2 bubble capture and absorption into the superaerophilic low-phi surface. Scalebar is 5 mm. (B) Comparison of average reaction rates across various surfaces tested, with low-phi spreading bubble case demonstrating a 2-orders-of-magnitude improvement over b5 micro-post textured surface, smooth Teflon, and smooth silicon capture surfaces. Reaction rates for surfaces other than low-phi represent the first 20 seconds of absorption, as bubbles reached a plateau in absorption and were not fully absorbed like in the low-phi case. (C) Comparison between average reaction rates for low-phi spreading bubble case measurements and model predictions, confirming the magnitude of improvement over non-spreading bubble cases. (D) Time-lapse, high-speed imaging of the smallest bubbles directly injected into a low-phi capture surface, showing complete absorption in ~1 ms, encouraging the development of small-scale, modular high-performance absorption using this surface-enhanced direct injection method. Scalebar is 1 mm. (E) Schematic representation of a needle array, as shown in (D), to create a modular version of the surface-enhanced direct injection absorption system (left). On the right, volumetrically normalized reaction rates account for the absorption reactor size, comparing the proposed small-scale surface-enhanced direct injection absorber to a commercial reference, Petra Nova's absorption tower, a large-scale post-combustion carbon capture facility in Texas, USA.

Rapid and Complete Absorption with Superhydrophobic Low-Phi Capture Surfaces

After fabricating and evaluating the nanoscale capture surfaces' ability to spread air bubbles, we examined their potential for enhancing CO_2 bubble absorption using a 0.1 M KOH absorption solution. Owing to the similar performance of both ng and low-phi surfaces, we selected the hierarchical low-phi surface for absorption testing due to its ease of fabrication via laser ablation and its capacity to hold more gas within its deeper, hierarchical texture compared to the purely nanoscale ng surfaces. High-speed imaging revealed rapid capture and full spreading of the

CO_2 bubble within approximately 10 ms, during which it was absorbed while reacting with the hydroxide solution to form potassium bicarbonate. Crucially, the absorption timescale was reduced from tens of seconds for a similarly sized captive bubble to about 100 ms for complete absorption in the spreading case. Consequently, the average reaction rate for these bubbles was about two orders of magnitude higher than the average reaction rates for the first 20 seconds for captive bubbles tested on all non-nanoscale capture surfaces, as shown in Figure 4B. This increased reaction rate magnitude is accurately captured by the developed model, which predicts a two-order increase relative to the non-spreading bubble case, as illustrated in Figure 4C. The enhanced CO_2 absorption is enabled by matching the bubble spreading timescale with the reaction timescale. The reaction timescale can be derived from the bulk concentration of reactant in solution and the reaction rate coefficient $\tau_{rxn} \sim (c_{bulk,\,OH^-}\, k)^{-1} \approx 1.7\, ms$. Comparing this with the spreading timescale from the previous section results in a modified Damköhler number, Da, which represents a dimensionless number comparing the bubble spreading timescale with the reaction timescale:

$$Da = \frac{\tau_{spreading}}{\tau_{rxn}}$$

In our case, matching the spreading and reaction timescales between 1 and 10 ms enables continuous CO_2 supply to a new reacting gas-liquid interface, minimizing and resetting the diffusion boundary layer. This minimization allows the reaction to proceed at the highest rates while the bubble spreads. Additionally, the spreading increases the gas surface area per volume available for reaction compared to a spherical bubble, maintaining a relatively constant enlarged surface area for interaction after the bubble has spread into the texture. This is advantageous compared to a shrinking bubble during absorption, which has its surface area decrease as the square of the bubble radius. Lastly, the rapid complete reaction of CO_2 with hydroxide allows the bubble

to be fully absorbed without the plateauing behavior observed in all non-spreading cases tested. The reaction occurs faster than product aggregation at the bubble interface, enabling the spreading bubble to react quickly enough to avoid product aggregation and be completely absorbed.

Interestingly, there is a reversal in the overall trend in average reaction rates and initial bubble size between the spreading and non-spreading bubble cases. For all non-spreading bubble capture surfaces tested, larger bubbles generally have higher absorption rates due to their larger available reaction area compared to smaller bubbles, as shown in Figure 4B. However, this tendency reverses for spreading bubble absorption, with the highest reaction rates observed for the smallest bubbles. Spreading significantly increases the surface area of these smaller bubbles, and their smaller gas volume allows them to react quickly enough to minimize diffusion boundary development relative to their larger spreading counterparts, resulting in rapid absorption. For instance, Figure 4D shows a bubble with a radius of approximately 500 μm being absorbed rapidly within just a few milliseconds, with successive bubbles injected at this rate over time.

A conceptual representation of an application for surface-enhanced direct gas injection for absorption is depicted in Figure 4E. An array of small needles rapidly injects gas bubbles into the capture surface, as illustrated in Figure 4E (left), spaced far enough apart to prevent significant interactions between neighboring spreading bubbles. A small-scale absorber of this type, with a 20 x 20 array of injection needles (400 total needles), would require dimensions of approximately 10 cm x 10 cm x 2.5 cm. Normalizing the average rate for this absorber by the reactor volume yields a reactor volumetric average reaction rate of ~1 kg/s/m³, as shown in Figure 4E (right). For comparison, we reference Petra Nova, one of the world's largest post-combustion carbon capture projects. Its absorption tower, which captures CO_2 from the exhaust of a nearby coal-fired power plant near Houston, Texas, has an annual capacity of 1.6 Mt CO_2[45]. The tower represents the

epitome of large-scale absorption tower advantages for gas separation. However, scaling down these technologies is challenging, making them unsuitable for distributed or small-scale, modular absorption applications. The surface-enhanced direct injection modality demonstrated here offers potential advantages for distributed and small-scale, modular operations. The volumetrically normalized average reaction rate for Petra Nova is approximately three orders of magnitude lower than that of the surface-enhanced direct injection embodiment envisioned here.

This comparison is intended to highlight the potential benefits of a surface-enhanced direct injection approach for high-performance, small-scale absorbers, not to suggest replacing existing large-scale absorption tower systems. In reality, the absorption demonstrated here, using pure CO_2 gas absorbed by a moderately alkaline KOH solution, cannot be directly compared to Petra Nova, where a gas mixture is treated with an amine-based absorber liquid at elevated temperature and pressure. However, the enhanced reaction rates achieved here with a relatively moderate KOH concentration of 0.1 M could be advantageous compared to higher concentration absorber units that risk material corrosion and damage in more alkaline environments, requiring stricter material considerations. Future research should extend the systems and tests demonstrated here to include multi-component gas mixtures instead of pure gas to increase the application relevance for industrial absorption units in separations and chemical scrubbing.

CONCLUSION

In conclusion, we have experimentally demonstrated and numerically modeled the enhancement of CO_2 bubble absorption by utilizing advantageous surface interactions to spread the bubble onto nanoengineered superhydrophobic bubble capture surfaces. This approach has increased the average reaction rates for the CO_2 absorption process by over two orders of magnitude compared to a non-spread bubble case. The critical importance of nanoscale surface roughness was showcased, and surfaces capable of fully spreading CO_2 bubbles on a timescale compatible with the absorption reaction timescale were presented.

Interestingly, non-spreading bubbles generally exhibit smaller reaction rates for smaller bubbles due to reduced surface area, but spreading bubbles reverse this trend. The smallest spreading bubbles displayed the highest average reaction rates for complete absorption, as their small volumes spread to large surface areas. All spreading bubbles facilitated complete absorption of the gas, avoiding the "plateauing" effect observed for all non-spreading bubbles and blisters tested.

Lastly, direct injection of gas bubbles was proposed as a potentially advantageous method for absorption compared to large-scale absorption towers on a volumetric basis. This concept encourages the use of this type of approach for modular and distributed absorption applications, where centralized large-scale absorption methods may not be practically or economically feasible.

SUPPORTING INFORMATION

Materials

For all carbon dioxide absorption experiments, the following materials were used for reactants: 0.1 M KOH solution was made mixing semiconductor grade (99.99% pure) potassium hydroxide pellets purchased from Sigma-Aldrich (Cat No: 306568) with ASTM Type I deionized water (18 MΩ-cm resistivity), pure carbon dioxide gas (99.995%) used for all experiments was purchased from Airgas (Cat No: CD PC200).

Bubble Image Segmentation & Analysis

The *Fiji* distribution of the image processing platform *ImageJ* was used for segmenting collected imaging data to arrive at binary segmented images of the bubbles from each analyzed frame. Briefly, a bounding box was drawn around the region of interest containing the full extent of the bubble to be segmented. Following this, the image area outside the relevant bounding box was cleared, and the image was binarized using *ImageJ's Make Binary* command, followed by the *ImageJ's Fill Holes* command. The resulting image was a binary image with the bubble representing the dark foreground and a white background surrounding the segmented bubble. These binary images were then processed using a MATLAB script to determine their volumes by assuming radial symmetry about the vertical midpoint of the captive bubble and revolving each radial row of radial pixels to achieve a volume. An *ImageJ* macro was recorded to make implementing this image processing workflow less time consuming, only requiring the bounding box location as an input and then being able to run on sequential images for a given sequence of data to collect time series trends for bubble volumes. Image processing was only utilized for analysis of non-spreading bubble imaging data.

Numerical Modeling

The following information includes additional reference information for physical constants and material properties used in modeling the results presented in manuscript, as well as data to highlight the fidelity of the model from a comparison with prior literature and convergence study results for temporal and spatial meshing using in MATLAB to accurately approximate spatial and temporal results.

Table S1: A table of physical constants and material properties used in the numerical model.

Constant	Value	Units
R	8.315	J/mol/K
T	293	K
P	101325	Pa
k	5.9	$m^3/mol/s$
D_{CO2}	1.96e-9	m^2/s
D_{OH}	6.8e-9	m^2/s
H_{CO2}	3.87e-4	$mol/m^3/Pa$
$C_{0,\,OH}$	100	mol/m^3

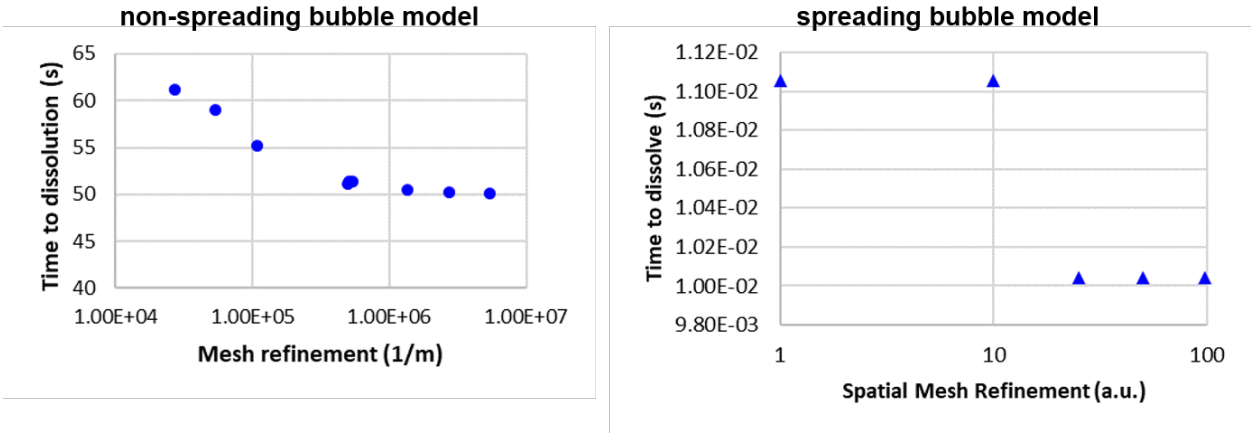

Figure S 1. Convergence of bubble dissolution time via spatial mesh refinement was confirmed for both spherical (left, non-spreading bubble model) and planar (right, spreading bubble model) geometries

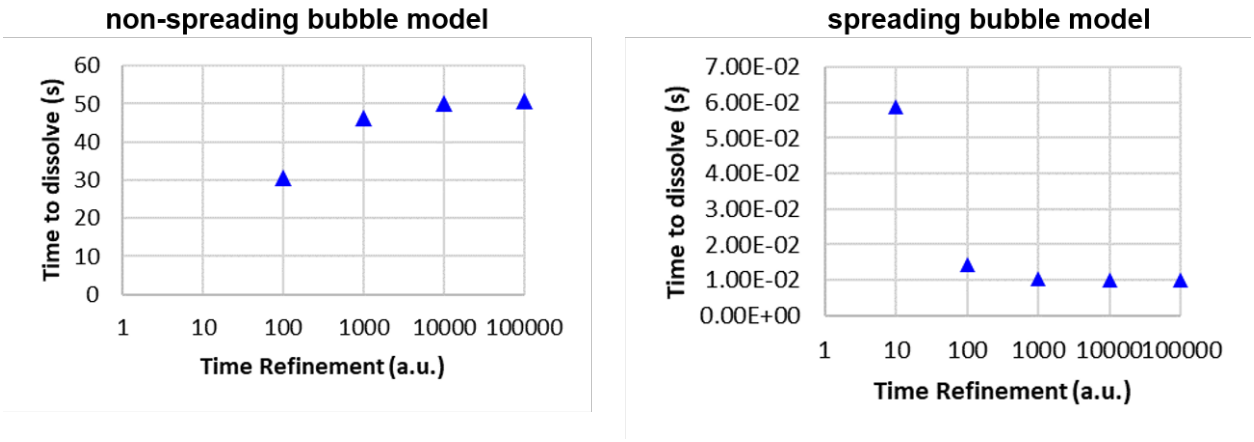

Figure S 2. Convergence of bubble dissolution time via temporal mesh refinement was confirmed for both spherical (left, non-spreading bubble model) and planar (right, spreading bubble model) geometries

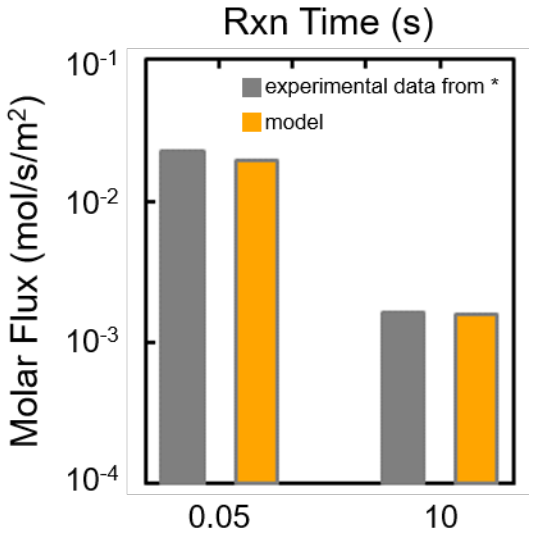

Figure S 3. Molar flux from solution of the model developed is in high agreement with literature values from previously published textbook for short reaction times of 0.05 s and long reaction times of 10 s. Reference for data comparison from * Sherwood, T. K., Pigford, R. L., & Wilke, C. R. (1975). *Mass Transfer*. McGraw-Hill.

Experimental & Imaging Setup

Imaging data for non-spreading captive bubbles was collected at 30 frames per second as videos using a DSLR camera (Nikon D800) and high magnification lens (Navitar 12x Zoom). High-speed imaging data collected at higher frame rates was used to determine the average reaction rate for spreading bubbles, collected at 5,000 frames per second using a high-speed camera (Photron SA-1). For the embodiment shown of injection of the smallest bubbles tested, a higher frame of 40,000 frames per second was used to increase the temporal resolution of the data collection. The following figures show a photo of the experimental setup used to capture bubbles on a capture surface and image from the side profile, along with a schematic diagram of the setup used to enable single bubble control via using pressure regulated gas flow of CO_2 and precisely timed actuation of solenoid valves via a microcontroller to deposit a single bubble CO_2 on-demand.

Fabrication of Textured Capture Surfaces for Testing

Nanotexture, nanograss, "*ng*" capture surfaces are fabricated using a fluorine based reactive ion etching (RIE) process. Oxygen is introduced into the chamber during fluorine etching and causes for the formation of oxide precipitates which are deposited and subsequently etched to create the relatively random nanoscale features that produce the nanotexture of the "nanograss" texture that is achieved

Hierarchical "*low-phi*" capture surfaces are fabricated using a 1064 nm Nd:YAG laser (TYMKA Electrox) to ablate the surface of a polished silicon wafer. The ablation process was controlled to make a repeating raster pattern on the surface of the silicon which results in a hierarchical micro/nanotexture. The microscale pyramidal structures consisted of closely packed and reproducible pyramidal features spaced ~ 75 μm apart and 75 μm from the spacing between the raster pattern of the laser on the surface. The nanoscale roughness is created through the

thermal ablation process as the silicon is ablated from the surface, leaving a micro- / nanoscale hierarchical structure.

Microtextured "*b5*" capture surfaces were fabricated using a combination of photolithography and deep reactive ion etching processing (DRIE) to achieve a regular array of rectangular posts with a well-controlled spacing between them. In this case the microposts are 10 μm side lengths of the top square surface, 10 μm tall, and spaced 5 μm from adjacent microposts.

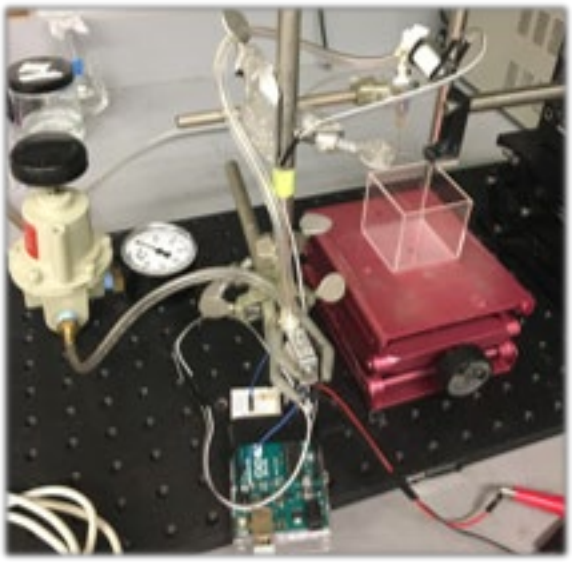

Figure S 4. Photo of experimental setup for delivering single bubbles to capture surfaces during experiments relevant for this work.

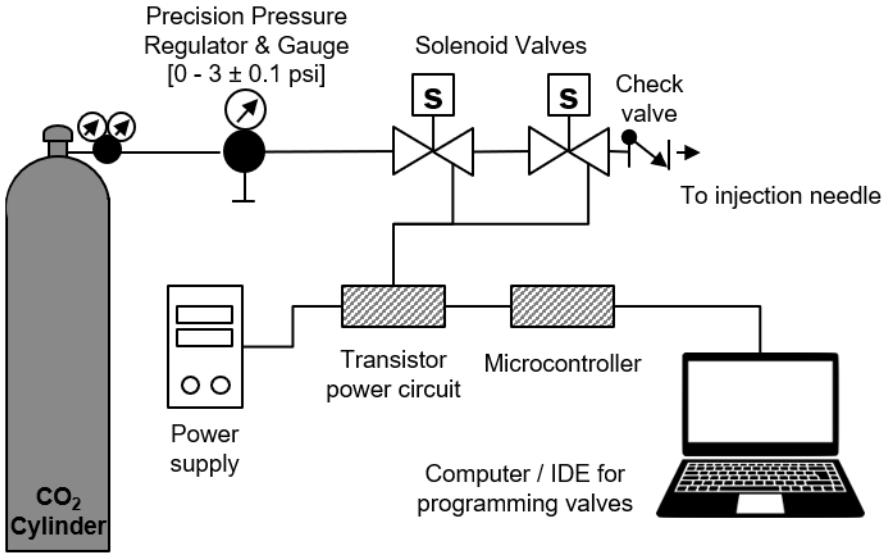

Figure S 5. Schematic illustration of the experimental setup used to inject single bubbles via pressure driven flow through an injection needle using a pair of solenoid valves controlled via a microcontroller.

REFERENCES

(1) Yildirim, Ö.; Kiss, A. A.; Hüser, N.; Leßmann, K.; Kenig, E. Y. Reactive Absorption in Chemical Process Industry: A Review on Current Activities. *Chemical Engineering Journal* **2012**, *213*, 371–391. https://doi.org/10.1016/J.CEJ.2012.09.121.

(2) Chen, L.; Lin, J. W.; Yang, C. L. Absorption of NO2 in a Packed Tower with Na2SO3 Aqueous Solution. *Environmental Progress* **2002**, *21* (4), 225–230. https://doi.org/10.1002/EP.670210411.

(3) Lin, C.-C.; Liu, W.-T.; Tan, C.-S. Removal of Carbon Dioxide by Absorption in a Rotating Packed Bed. **2003**. https://doi.org/10.1021/IE020669.

(4) Spedding, P. L.; Munro, P. A.; Jones, M. T. Ammonia Absorption into Water in a Packed Tower I: Characterization of Packing and Liquid Distribution. *The Chemical Engineering Journal* **1986**, *32* (2), 65–76. https://doi.org/10.1016/0300-9467(86)80053-3.

(5) Zarzycki, R.; Chacuk, A. *Absorption: Fundamentals & Applications*; 2013.

(6) F Delvigne; JP Lecomte. *Encyclopedia on Industrial Biotechnology: Bioprocess, Bioseparation and Cell Technologies. Foam Formation and Control in Bioreactors*; Wiley: New York, NY, 2010.

(7) Chalmers, J. J.; Bavarian, F. Microscopic Visualization of Insect Cell-Bubble Interactions. II: The Bubble Film and Bubble Rupture. *Biotechnol Prog* **1991**, *7* (2), 151–158. https://doi.org/10.1021/BP00008A010.

(8) Cherry, R. S.; Hulle, C. T. Cell Death in the Thin Films of Bursting Bubbles. *Biotechnol Prog* **1992**, *8* (1), 11–18. https://doi.org/10.1021/BP00013A003.

(9) Betts, J. I.; Baganz, F. Miniature Bioreactors: Current Practices and Future Opportunities. *Microb Cell Fact* **2006**, *5* (1), 1–14. https://doi.org/10.1186/1475-2859-5-21/FIGURES/3.

(10) Gupta, P. L.; Lee, S. M.; Choi, H. J. A Mini Review: Photobioreactors for Large Scale Algal Cultivation. *World J Microbiol Biotechnol* **2015**, *31* (9), 1409–1417. https://doi.org/10.1007/S11274-015-1892-4/FIGURES/5.

(11) Langley, N. M.; Harrison, S. T. L.; van Hille, R. P. A Critical Evaluation of CO2 Supplementation to Algal Systems by Direct Injection. *Biochem Eng J* **2012**, *68*, 70–75. https://doi.org/10.1016/J.BEJ.2012.07.013.

(12) *Global Defoamers Market Size & Share Report, 2030*. https://www.grandviewresearch.com/industry-analysis/defoamers-market (accessed 2022-09-27).

(13) Deotale, S.; Dutta, S.; Moses, J. A.; Balasubramaniam, V. M.; Anandharamakrishnan, C. Foaming Characteristics of Beverages and Its Relevance to Food Processing. *Food Engineering Reviews* **2020**, *12* (2), 229–250. https://doi.org/10.1007/S12393-020-09213-4/FIGURES/10.

(14) Wang, L. K. Humanitarian Engineering Education of the Lenox Institute of Water Technology and Its New Potable Water Flotation Processes. **2021**, 1–72. https://doi.org/10.1007/978-3-030-54642-7_1.

(15) Li, P.; Wu, Q.; Wu, H.; Wen, S.; Wang, L.; Li, S. Flocculation-Air Flotation Treatment of Wastewater from Paper-Making Reconstituted Tobacco Sheet. *IOP Conf. Series: Earth and Environmental Science* **2018**, *170* (032082). https://doi.org/10.1088/1755-1315/170/3/032082.

(16) Lim, K.; Evans, P. J.; Parameswaran, P. Long-Term Performance of a Pilot-Scale Gas-Sparged Anaerobic Membrane Bioreactor under Ambient Temperatures for Holistic Wastewater Treatment. *Environ Sci Technol* **2019**, *53* (13), 7347–7354. https://doi.org/10.1021/ACS.EST.8B06198/ASSET/IMAGES/LARGE/ES-2018-061989_0004.JPEG.

(17) Vyrides, I.; Stuckey, D. C. Saline Sewage Treatment Using a Submerged Anaerobic Membrane Reactor (SAMBR): Effects of Activated Carbon Addition and Biogas-Sparging Time. *Water Res* **2009**, *43* (4), 933–942. https://doi.org/10.1016/J.WATRES.2008.11.054.

(18) Takemura, F.; Matsumoto, Y. Dissolution Rate of Spherical Carbon Dioxide Bubbles in Strong Alkaline Solutions. *Chem Eng Sci* **2000**, *55* (18), 3907–3917. https://doi.org/10.1016/S0009-2509(00)00022-1.

(19) Sherwood, T. K. *Absorption and Extraction*, 1st ed.; McGraw-Hill Book Co.: New York, NY, 1937.

(20) Sherwood, T. K.; Pigford, R. L.; Wilke, C. R. *Mass Transfer*; McGraw-Hill: New York, NY, 1975.

(21) Abanades, J. C.; Arias, B.; Lyngfelt, A.; Mattisson, T.; Wiley, D. E.; Li, H.; Ho, M. T.; Mangano, E.; Brandani, S. Emerging CO2 Capture Systems. *International Journal of Greenhouse Gas Control* **2015**, *40*, 126–166. https://doi.org/10.1016/J.IJGGC.2015.04.018.

(22) Keith, D. W.; Holmes, G.; st. Angelo, D.; Heidel, K. A Process for Capturing CO2 from the Atmosphere. *Joule* **2018**, *2* (8), 1573–1594. https://doi.org/10.1016/J.JOULE.2018.05.006.

(23) Bushuyev, O. S.; de Luna, P.; Dinh, C. T.; Tao, L.; Saur, G.; van de Lagemaat, J.; Kelley, S. O.; Sargent, E. H. What Should We Make with CO2 and How Can We Make It? *Joule* **2018**, *2* (5), 825–832. https://doi.org/10.1016/j.joule.2017.09.003.

(24) Rahman, F. A.; Aziz, M. M. A.; Saidur, R.; Bakar, W. A. W. A.; Hainin, M. R.; Putrajaya, R.; Hassan, N. A. Pollution to Solution: Capture and Sequestration of Carbon Dioxide (CO2) and Its Utilization as a Renewable Energy Source for a Sustainable Future. *Renewable and Sustainable Energy Reviews* **2017**, *71*, 112–126. https://doi.org/10.1016/J.RSER.2017.01.011.

(25) Yu, C. H.; Huang, C. H.; Tan, C. S. A Review of CO2 Capture by Absorption and Adsorption. *Aerosol Air Qual Res* **2012**, *12* (5), 745–769. https://doi.org/10.4209/AAQR.2012.05.0132.

(26) Diederichsen, K. M.; Sharifian, R.; Kang, J. S.; Liu, Y.; Kim, S.; Gallant, B. M.; Vermaas, D.; Hatton, T. A. Electrochemical Methods for Carbon Dioxide Separations. *Nature Reviews Methods Primers 2022 2:1* **2022**, *2* (1), 1–20. https://doi.org/10.1038/s43586-022-00148-0.

(27) Naraharisetti, P. K.; Yeo, T. Y.; Bu, J. New Classification of CO2 Mineralization Processes and Economic Evaluation. *Renewable and Sustainable Energy Reviews* **2019**, *99*, 220–233. https://doi.org/10.1016/J.RSER.2018.10.008.

(28) Geerlings, H.; Zevenhoven, R. CO2 Mineralization—Bridge Between Storage and Utilization of CO2. *http://dx.doi.org/10.1146/annurev-chembioeng-062011-080951* **2013**, *4*, 103–117. https://doi.org/10.1146/ANNUREV-CHEMBIOENG-062011-080951.

(29) Pan, S. Y.; Chen, Y. H.; Fan, L. S.; Kim, H.; Gao, X.; Ling, T. C.; Chiang, P. C.; Pei, S. L.; Gu, G. CO2 Mineralization and Utilization by Alkaline Solid Wastes for Potential Carbon Reduction. *Nature Sustainability 2020 3:5* **2020**, *3* (5), 399–405. https://doi.org/10.1038/s41893-020-0486-9.

(30) Xie, H.; Yue, H.; Zhu, J.; Liang, B.; Li, C.; Wang, Y.; Xie, L.; Zhou, X. Scientific and Engineering Progress in CO2 Mineralization Using Industrial Waste and Natural Minerals. *Engineering* **2015**, *1* (1), 150–157. https://doi.org/10.15302/J-ENG-2015017.

(31) la Plante, E. C.; Simonetti, D. A.; Wang, J.; Al-Turki, A.; Chen, X.; Jassby, D.; Sant, G. N. Saline Water-Based Mineralization Pathway for Gigatonne-Scale CO2 Management. *ACS Sustain Chem Eng* **2021**, *9* (3), 1073–1089. https://doi.org/10.1021/ACSSUSCHEMENG.0C08561/ASSET/IMAGES/LARGE/SC0C08561_0007.JPEG.

(32) Zhang, S.; DePaolo, D. J. Rates of CO2 Mineralization in Geological Carbon Storage. *Acc Chem Res* **2017**, *50* (9), 2075–2084. https://doi.org/10.1021/ACS.ACCOUNTS.7B00334/ASSET/IMAGES/AR-2017-00334D_M007.GIF.

(33) Rubino, J. G.; Velis, D. R.; Sacchi, M. D. Numerical Analysis of Wave-Induced Fluid Flow Effects on Seismic Data: Application to Monitoring of CO2 Storage at the Sleipner Field. *J Geophys Res Solid Earth* **2011**, *116* (B3), 3306. https://doi.org/10.1029/2010JB007997.

(34) Trias, R.; Ménez, B.; le Campion, P.; Zivanovic, Y.; Lecourt, L.; Lecoeuvre, A.; Schmitt-Kopplin, P.; Uhl, J.; Gislason, S. R.; Alfreosson, H. A.; Mesfin, K. G.; Snæbjörnsdóttir, S. O.; Aradóttir, E. S.; Gunnarsson, I.; Matter, J. M.; Stute, M.; Oelkers, E. H.; Gérard, E. High Reactivity of Deep Biota under Anthropogenic CO2 Injection into Basalt. *Nature Communications 2017 8:1* **2017**, *8* (1), 1–14. https://doi.org/10.1038/s41467-017-01288-8.

(35) Pogge von Strandmann, P. A. E.; Burton, K. W.; Snæbjörnsdóttir, S. O.; Sigfússon, B.; Aradóttir, E. S.; Gunnarsson, I.; Alfredsson, H. A.; Mesfin, K. G.; Oelkers, E. H.; Gislason,

S. R. Rapid CO2 Mineralisation into Calcite at the CarbFix Storage Site Quantified Using Calcium Isotopes. *Nature Communications 2019 10:1* **2019**, *10* (1), 1–7. https://doi.org/10.1038/s41467-019-10003-8.

(36) Snæbjörnsdóttir, S.; Sigfússon, B.; Marieni, C.; Goldberg, D.; Gislason, S. R.; Oelkers, E. H. Carbon Dioxide Storage through Mineral Carbonation. *Nature Reviews Earth & Environment 2020 1:2* **2020**, *1* (2), 90–102. https://doi.org/10.1038/s43017-019-0011-8.

(37) Matter, J. M.; Stute, M.; Snæbjörnsdottir, S.; Oelkers, E. H.; Gislason, S. R.; Aradottir, E. S.; Sigfusson, B.; Gunnarsson, I.; Sigurdardottir, H.; Gunnlaugsson, E.; Axelsson, G.; Alfredsson, H. A.; Wolff-Boenisch, D.; Mesfin, K.; Taya, D. F. D. L. R.; Hall, J.; Dideriksen, K.; Broecker, W. S. Rapid Carbon Mineralization for Permanent Disposal of Anthropogenic Carbon Dioxide Emissions. *Science (1979)* **2016**, *352* (6291), 1312–1314. https://doi.org/10.1126/SCIENCE.AAD8132/SUPPL_FILE/AAD8132-MATTER-SM.PDF.

(38) Shojai Kaveh, N.; Rudolph, E. S. J.; van Hemert, P.; Rossen, W. R.; Wolf, K. H. Wettability Evaluation of a CO2/Water/Bentheimer Sandstone System: Contact Angle, Dissolution, and Bubble Size. *Energy and Fuels* **2014**, *28* (6), 4002–4020. https://doi.org/10.1021/EF500034J/ASSET/IMAGES/EF-2014-00034J_M028.GIF.

(39) de Maleprade, H.; Clanet, C.; Quéré, D. Spreading of Bubbles after Contacting the Lower Side of an Aerophilic Slide Immersed in Water. *Phys Rev Lett* **2016**, *117* (9), 094501. https://doi.org/10.1103/PHYSREVLETT.117.094501/FIGURES/4/MEDIUM.

(40) Rapoport, L.; Emmerich, T.; Varanasi, K. K.; Rapoport, L.; Emmerich, T.; Varanasi, K. K. Capturing Bubbles and Preventing Foam Using Aerophilic Surfaces. *Adv Mater Interfaces* **2020**, *7* (6), 1901599. https://doi.org/10.1002/ADMI.201901599.

(41) Davis, H. S.; Crandall, G. S. The Role of the Liquid Stationary Film in Batch Absorptions of Gases. II. Absorptions Involving Irreversible Chemical Reactions. *The Liquid Stationary Film in Gas Absorptions* **1930**, *52*, 3769.

(42) Hitchcock, L. B. Rate of Absorption of Carbon Dioxide Effect of Concentration and Viscosity of Caustic Solutions. *Ind Eng Chem* **1934**, *25* (11), 1158–1167.

(43) Vassilatos, G.; Trass, O.; Johnson, A. I. Simultaneous Gas Absorption and Liquid Phase Chemical Reaction in an Agitated Vessel. *Can J Chem Eng* **1962**, *40* (5), 210–214. https://doi.org/10.1002/CJCE.5450400507.

(44) Schennetten, K.; Meier, M. M.; Scheibinger, M. Non-Sticking Drops. *Reports on Progress in Physics* **2005**, *68* (11), 2495. https://doi.org/10.1088/0034-4885/68/11/R01.

(45) NRG Energy Inc. *NRG Investor Presentation*. https://investors.nrg.com/static-files/5959d26c-3a5f-4fe6-9cdb-f7c07bf1d4b7 (accessed 2022-09-28).